Lab on a Chip

PAPER

View Article Online
View Journal | View Issue

Feedback control of inertial microfluidics using axial control forces†

Cite this: *Lab Chip*, 2014, **14**, 2115

Christopher Prohm* and Holger Stark

Inertial microfluidics is a promising tool for many lab-on-a-chip applications. Particles in channel flows with Reynolds numbers above one undergo cross-streamline migration to a discrete set of equilibrium positions in square and rectangular channel cross sections. This effect has been used extensively for particle sorting and the analysis of particle properties. Using the lattice Boltzmann method, we determined the equilibrium positions in square and rectangular cross sections and classify their types of stability for different Reynolds numbers, particle sizes, and channel aspect ratios. Our findings thereby help to design microfluidic channels for particle sorting. Furthermore, we demonstrated how an axial control force, which slows down the particles and shifts the stable equilibrium position towards the channel center. Ultimately, the particles then stay on the centerline for forces exceeding the threshold value. This effect is sensitive to the particle size and channel Reynolds number and therefore suggests an efficient method for particle separation. In combination with a hysteretic feedback scheme, we can even increase the particle throughput.

Received 3rd February 2014,
Accepted 24th March 2014

DOI: 10.1039/c4lc00145a

www.rsc.org/loc

1. Introduction

In recent years, a number of devices using fluid inertia in microfluidic setups have been proposed for applications such as particle steering and sorting or for the whole range of flow cytometric tasks in biomedical applications. They include cell counting, cell sorting, and mechanical phenotyping.[1–4] These devices rely on cross-streamline migration of solute particles subjected to fluid flow where fluid inertia cannot be neglected as is commonly done in microfluidics. In this article we have demonstrated how control forces along the channel axis influence inertial cross-streamline migration and how feedback control using axial forces enhances particle throughput.

Segré and Silberberg, who investigated colloidal particles in circular channels, were the first to attribute cross-streamline migration to fluid inertia.[5] They observed that flowing particles gathered on a circular annulus about halfway between the channel center and the wall. This effect is connected to an inertial lift force in the radial direction. It becomes zero right on the annulus which marks degenerate stable equilibrium positions in the circular cross section. For microfluidic applications, channels with a rectangular cross section are used since they can be fabricated more easily. The reduced symmetry qualitatively changes the lift force profile and only a discrete set of equilibrium positions remain.[6] In square channels, they are typically found halfway between the channel center and the centers of the channel walls.[7] In numerical studies, migration to positions on the diagonals are also observed.[8,9] In rectangular channels, the number of equilibrium positions is further reduced to two when the aspect ratio strongly deviates from one.[1,10] The particles all gather in front of the long channel walls. The exact equilibrium positions are of special importance, as they ultimately determine how devices function based on inertial microfluidics.[1–3]

Inertial lift forces that drive particles away from the channel center are caused by the non-zero curvature or the parabolic shape of the Poiseuille flow profile.[6,11] Only close to the channel walls, wall-induced lift forces push particles towards the center. In channels with a rectangular cross section, the curvature of the flow profile is strongly modified. Along the short main axis, the flow profile remains approximately parabolic, while along the long main axis it almost assumes the shape of a plug flow with strongly reduced curvature in the center when the cross section is strongly elongated.[12] The large difference in curvature along the two main axes modifies the lift force profiles in both directions.[6] We will investigate them in more detail in this article.

The method of matched asymptotic expansion allows an analytic treatment of inertia-induced migration and calculation of the lift force profiles.[13,14] As the method requires the particle radius to be much smaller than the channel diameter, it is hardly applicable to microfluidic particle flow, where this assumption is often violated. Here, numerical approaches provide further insight. Previous studies in three dimensions

Institute of Theoretical Physics, Technische Universität Berlin, Hardenbergstr. 36, 10623 Berlin, Germany. E-mail: Christopher.Prohm@TU-Berlin.de

† Electronic supplementary information (ESI) available: Includes a summary of the lattice Boltzmann method and the implementation of the Inamuro immersed boundary method. See DOI: 10.1039/c4lc00145a

have used the lattice Boltzmann method,[9] the finite element method,[6] or multi-particle collision dynamics.[15]

Using additional control methods such as optical lattices[16] or optimal control[17] can increase the efficiency of microfluidic devices. In an attractive experiment, Kim and Yoo demonstrated a method to focus particles to the channel center.[18] They applied an electric field along the channel axis to slow down the particles relative to the external Poiseuille flow, which induces a Saffmann force towards the channel center.[19] The experiments were performed at Reynolds number Re $\approx$ 0.05. We will take up this idea and study, at moderate Reynolds numbers, how the inertial lift force profile changes under an axial control force.

A more sophisticated method to operate a system is feedback control where the control action depends on the current state. It is widely used in engineering and everyday life.[20] In microfluidic systems, optical tweezers combined with feedback control provide a strategy to measure microscopic forces in polymers and molecular motors.[21–23] In lab-on-a-chip devices, several strategies are suggested for sorting particles. They all monitor particle flow directly and use the recorded signal to implement feedback-controlled optical manipulation.[24–26] We will apply a simple form of feedback control to keep the particles in the channel center.

In this paper, we use the lattice Boltzmann method to investigate several aspects of inertial microfluidics. We study in detail the equilibrium particle positions in microfluidic channels with square and rectangular cross sections and categorize their types of stability. In particular, we show how, for channels with sufficiently elongated cross sections, colloidal particles are constrained to move in a plane. We also show how the inertial lift force profile is manipulated by applying an axial control force such that the stable equilibrium position gradually moves to the channel center. The effect strongly depends on the particle size and therefore can be applied for particle sorting. Finally, using the axial force, we implement hysteretic feedback control to keep the particle close to the channel center and demonstrate how this enhances particle throughput compared to the case of constant forcing. In the conclusions, we refer to the experiments of Kim and Yoo[18] as potential experimental approaches to realize the axial feedback control.

The article is organized as follows: in sect. 2, we introduce the microfluidic geometry, explain details of the lattice Boltzmann implementation, and shortly introduce Langevin dynamics simulations; our results on equilibrium positions and lift-force profiles in square and rectangular channels are reported in sect. 3; we demonstrate the influence of axial control forces on the lift force profile in sect. 4; we combine it with feedback control in sect. 5; and we finish with the conclusions in sect. 6.

2 Methods

In this section, we first introduce the microfluidic system. We then shortly discuss the lattice Boltzmann method and refer to the details in the appendix. We introduce the procedure used to determine the inertial lift forces, and finally the Langevin dynamics for our feedback-control scheme.

2.1 Microfluidic system

We investigated a microfluidic channel with a rectangular cross section of height $2h$, width $2w$, and length L as illustrated in Fig. 1. We chose the coordinate system such that the z axis coincides with the channel axis and the x and y axes define the horizontal and vertical directions in the cross section, respectively. The channel center corresponds to $x = y = 0$. The channel was filled by a Newtonian fluid with density ρ and kinematic viscosity ν and a pressure driven Poiseuille flow was applied.[12] The maximum flow velocity u_0 at the channel center determines the Reynolds number Re = $2wu_0/\nu$. The implementation of the Poiseuille flow within the lattice Boltzmann method will be discussed in the next section.

Inside the channel, we placed a neutrally buoyant colloid with radius a. It follows the streamlines of the applied Poiseuille flow with an axial velocity v_z close the external Poiseuille flow velocity. Due to the fluid inertia the colloidal particle experiences a lateral lift force f_{lift}, which leads to cross-streamline migration. In sects. 4 and 5, we also applied an additional axial control force f_{ctl} to the colloidal particle. We used periodic boundary conditions along the axial direction and a channel length $L = 20a$ to ensure that the periodic colloidal images do not interact with each other and thereby do not influence our results.

2.2 The lattice Boltzmann method

We used the lattice Boltzmann method (LBM) to solve the Navier–Stokes equations of a Newtonian fluid.[27,28] LBM employs an ensemble of point particles that perform alternating steps of free streaming and collisions. The particles are constrained to move on a cubic lattice with a lattice spacing Δx. This restricts the particle velocities to a discrete set of vectors $\vec{c}_i$ such that after each streaming step with duration Δt the new particle positions again lie on the lattice. In LBM, one describes the

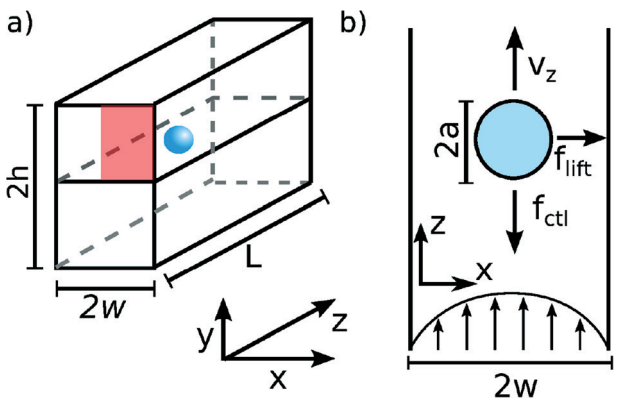

Fig. 1 A schematic of the microfluidic channel (a) and the xz plane at $y = 0$ (b). Further explanations are given in the main text. It is sufficient to only determine the inertial lift force f_{lift} in the red quadrant due to the symmetry of the rectangular cross section.

number of particles at lattice point $\vec{x}$ with velocity $\vec{c}_i$ by the distribution function $f_i(\vec{x},t)$. The first two moments of this distribution function give the hydrodynamic variables: number density $\rho(\vec{x},t)=\sum_i f_i(\vec{x},t)$ and velocity $\vec{u}(\vec{x},t)=\frac{1}{\rho}\sum_i \vec{c}_i f_i(\vec{x},t)$. Further details of our implementation are found in sect. S1 of the ESI.†

We implemented the pressure driven Poiseuille flow by imposing a constant body force $\vec{g}$ on the fluid such that the fluid velocity $\vec{u}(\vec{x},t)$ used to calculate the equilibrium distribution f_i^{eq} (see ESI†) is replaced by[29]

$$\vec{u} \to \vec{u} + \tau \vec{g}. \quad (1)$$

We confirmed as shown in Fig. 2 that this procedure does indeed reproduce the analytically known Poiseuille flow profile.

We placed a colloid in the Poiseuille flow and studied its position $\vec{r}$, velocity $\vec{v}$, and angular velocity $\vec{\omega}$. We combined the colloid to the fluid using the Inamuro Immersed Boundary (IB) method[30] with "five iterations". For reference, we presented a short summary of our implementation in sect. S2 of the ESI.†

We used the palabos LB code[31] to implement the LB algorithm. We modified the immersed boundary (IB) algorithm to correctly account for the periodic boundary conditions along the channel axis and implemented the colloid dynamics according to eqn (S9) in the ESI.†

Along the channel width, we used a total of 101 lattice sites including the boundaries. We implemented a cubic simulation grid and chose the number of lattice sites in the other two directions accordingly. We chose the maximum flow velocity in the channel such that the Mach number satisfies Ma = $u_{max}/c_s \leq 0.1$. Finally, we adjusted the kinematic viscosity by the relaxation time τ and thereby fixed the desired Reynolds number Re = $u_{max}w/\nu$. When $\tau > 1$, we readjusted the Mach number such that $\tau = 1$, as it has been shown that the accuracy of the combined LBM-IB methods greatly decreases for relaxation times larger than one.[32,33]

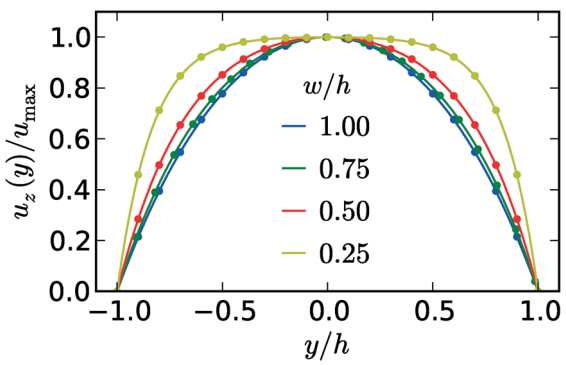

Fig. 2 Velocity profiles of the Poiseuille flow in the rectangular channel plotted at $x = 0$ along the y axis (the long cross sectional axis) for different aspect ratios w/h. The solid lines show the analytical form of the profiles,[12] while the symbols show results of the LB simulations.

2.3 Determining inertial lift forces

To determine inertial lift forces from LB simulations, we constrained the colloid to a fixed lateral position by simply disregarding any colloid motion in the cross-sectional plane. However, we did not impose any constraints on the axial and rotational motions.

To speed up our simulations, we initialized the system with the analytical solution of the rectangular Poiseuille flow and gave the colloid an initial axial velocity $v_z = 0.8u_0$, where u_0 is the flow velocity at the channel center. Going through transient dynamics, the system relaxes rapidly into a unique steady state within the first 1000 time steps. We continued the time-evolution up to the vortex diffusion time $T = 0.5w^2/\nu$ and determined the inertial lift force by averaging the colloidal force $\vec{F}_{fluid}$ from eqn (S7) in the ESI† over the last 2000 time steps of the simulations. We demonstrated in previous studies[15,17] that this procedure does indeed reproduce correct lift-force profiles.

2.4 Langevin dynamics simulations

As demonstrated below, axial control forces influence the inertial lift-force profiles which we determined in the LB simulations. We then used these profiles in Langevin dynamics simulations of the colloidal motion to investigate the potential benefit of feedback control using axial control forces.

We restricted ourselves to channels with an aspect ratio $w/h = 1/3$, which ensures that the colloidal dynamics essentially takes place in the xz plane as discussed in sect. 3.2. As we will discuss in sect. 4, the inertial lift force f_{lift} and the axial velocity v_z depend on the applied axial control force f_{ctl}. We also included thermal noise to exploit the stability of the fix points of the colloidal motion under feedback control. Following our work in ref. 17, we only included thermal noise along the lateral direction, as the axial velocities are much larger than the lateral ones. Then, the Langevin equations of motion in the lateral and axial directions are given by

$$\xi \frac{\mathrm{d}}{\mathrm{d}t}x = f_{lift}(x, f_{ctl}) + \eta(t), \quad (2)$$

$$\frac{\mathrm{d}}{\mathrm{d}t}z = v_z(x, f_{ctl}), \quad (3)$$

where the white noise force has zero mean, $\langle\eta(t)\rangle = 0$, and its variance obeys the fluctuation–dissipation theorem, $\langle\eta(t)\eta(t')\rangle = 2k_BT\xi\delta(t-t')$. We solved the Langevin equations using the conventional Euler scheme.[34] The parameters were chosen for a channel with width $2w = 20$ μm and at temperature $T = 300$ K.

3. Inertial lift forces for different channel geometries

In channels with circular cross sections, inertial lift forces drive colloids to a circular annulus with a radius of about

half the channel radius. The axial symmetry is reduced in channels with square or rectangular cross sections and instead of an annulus, particles accumulate at a discrete set of stable equilibrium positions.[7] In addition, the system also shows unstable equilibrium positions, where the lift force also vanishes but particles migrate away from them upon a small disturbance.

In the following two sections, we will investigate the location and the stability of the equilibrium positions for different particle sizes, Reynolds numbers, and channel geometries. We will discuss in detail how we can tailor colloidal motion by varying the aspect ratio of the channel cross section. Due to symmetry, we can restrict our discussion to the upper right quadrant shown in Fig. 1. In Fig. 3, we show the forces acting on a particle with radius $a/w = 0.4$ and the resulting trajectories at Reynolds number Re = 10 for different channel cross sections. We will discuss the relevant features first for a channel with square cross sections and then for general rectangular cross sections.

3.1 Square channels

In a channel with a square cross section and at Reynolds number Re = 10, a particle with radius $a/w = 0.4$ experiences the inertial force profile shown in Fig. 3(a). The gray lines indicate possible trajectories followed by the particles, which are free to migrate. Stable and unstable equilibrium positions are also indicated. We observed that the migration roughly occurs in two steps. From the channel center and the channel walls, strong radial forces drive the particle onto an almost circular annulus at about $r \approx 0.4w$. Since the forces are strong, migration occurs very rapidly. Then, the particle slowly migrates along the annulus to its equilibrium position here situated on the diagonal direction.

Together with the channel center there are in total nine equilibrium positions or fix points in the channel cross section. Four of them are indicated in Fig. 3(a). The channel center is always unstable and the particle migrates away from it. There are four fix points along the diagonal axes and four along the main axes (x, y directions) of the channel cross section. We plotted their distances from the center *versus* the colloid radius for several Re as shown in Fig. 4 and also indicated their stability. The fix points along the diagonals are always positioned further away from the channel center as there is more space for the particle. Consistent with the previous results,[6,9,15] we observed how both types of equilibrium positions move closer towards the channel center with increasing particle size and decreasing Reynolds number. Most importantly, small particles at high Reynolds numbers have their stable equilibrium positions on the main axes, while larger particles at lower Reynolds number move to the equilibrium positions on the diagonals. This is a new result compared to previous treatments.[6,8,9]

In the literature, equilibrium positions in square channels have been reported along the main axes,[6] along the diagonals for large deformable drops[8] or on both axes.[9] In contrast to ref. 9 we observed that the particles move either to the diagonal equilibrium positions or to the fix points on the main axes but the equilibrium positions are never stable at the same time as illustrated in Fig. 4. It has been demonstrated in spiral channels with a trapezoidal cross section[3] that such

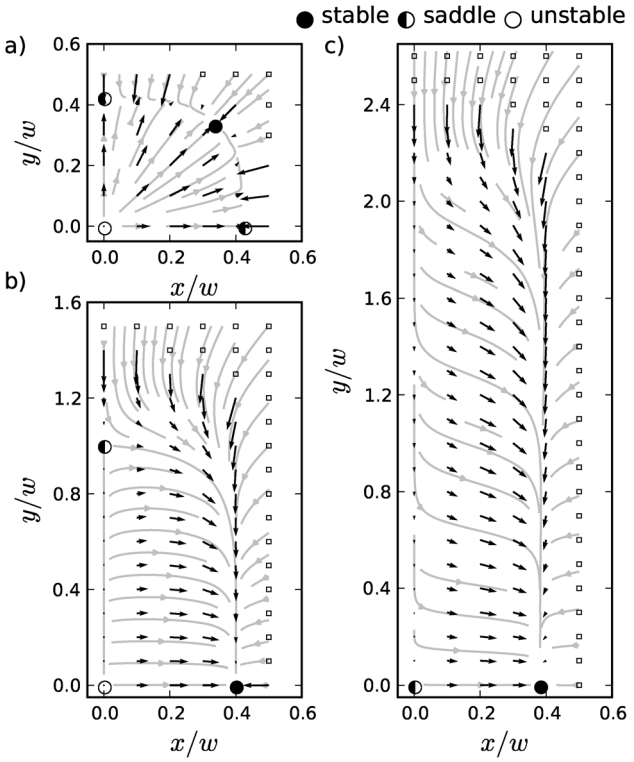

Fig. 3 Inertial lift forces (black arrows) of a colloidal particle with radius $a/w = 0.4$ in a pressure driven flow at Re = 10. The forces are plotted in the upper right quadrant of the microchannel cross section for aspect ratios $w/h = 1$ (a), $w/h = 1/2$ (b) and $w/h = 1/3$ (c). The gray lines indicate the trajectories of the colloidal particle as it experiences the lift forces. Lift forces larger than $0.35\rho v^2$ are not shown, as their positions are indicated by squares. Also indicated are the stable and unstable equilibrium positions. With "saddle" we denote the equilibrium positions unstable only along one direction.

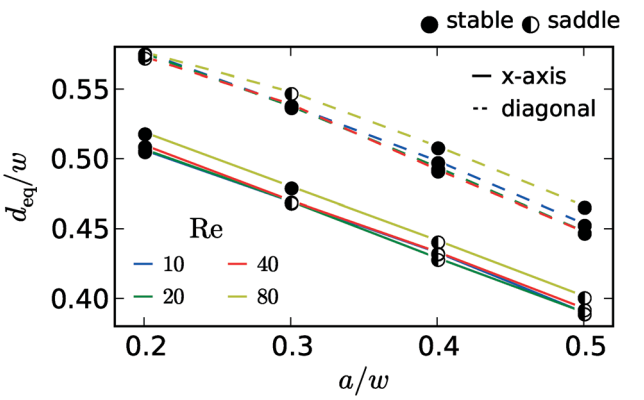

Fig. 4 Equilibrium positions d_{eq} (distance from the center) in a square channel are plotted *versus* the colloid radius for different Re. Equilibrium positions exist along the main axis in the x, y directions (solid lines) and along the diagonal (dashed line). Closed circles indicate stable equilibrium positions, whereas open circles are unstable.

a sudden change in stability can be used to efficiently sort particles by size. We noted that while the particle size is fixed by the specific system under investigation, the Reynolds number remains a free parameter and can be used to tune the stability of the equilibrium positions. Stable equilibrium positions on the diagonals were not observed in the experiments and finite element simulations performed by Di Carlo *et al.*[6] While we are not aware of any obvious reason how to resolve this discrepancy, we have noted that for channel aspect ratios different from unity a subtle change from stable diagonal equilibrium positions towards axial positions occurs as discussed in the next section. Furthermore, diagonal positions are only stable for sufficiently large particles.

3.2 Rectangular channels

In the experiments, channels typically with rectangular cross sections were used since the number of stable equilibrium positions reduces to two situated on the short main axis.[6] We observed the same behavior in the force profiles in Fig. 3 for large colloids, while for channels with a square cross section a particle migrates to its stable position on the diagonal [Fig. 3(a)], this fix point vanishes with a decreasing aspect ratio w/h and the stable equilibrium position switches to the short main axis along the x direction [Fig. 3(b)]. Further decreasing the aspect ratio w/h, the saddle fix point on the y axis vanishes completely and moves to the center at $x = y = 0$, where it keeps its stability along the y axis [Fig. 3(c)]. This has an important consequence (already exploited by us[17]) that the colloid is constrained to the xz plane at $y = 0$ and its dynamics becomes two-dimensional. In contrast, in Fig. 3(b), a particle starting close to the centerline moves out of the $y = 0$ plane on its way to the stable equilibrium position at $x \approx 0.4$. This is consistent with the simulations performed by Gossett *et al.*,[35] where a similar behavior was observed. We will now elaborate in more detail on these observations.

We first plotted the lift force along the y axis, *i.e.*, at $x = 0$ for several aspect ratios w/h as shown in Fig. 5. Due to symmetry, the lift force always points along the y direction. For the quadratic cross section, $w/h = 1$, zero lift forces indicate the unstable fix point in the center ($x = y = 0$) and the saddle fix point at $y \approx 0.42$, which is unstable in the x direction. As the channel cross section elongates along the y direction with decreasing w/h, the lift force driving the particle away from the channel center becomes weaker and the saddle fix point shifts towards the channel wall. Below the width $w \approx 0.45h$, the lift force close to the center becomes negative and the unstable fix point at $y = 0$ splits into a saddle fix point (now stable in the y direction) and an additional unstable fix point. While we did not show this situation in Fig. 3, it qualitatively looks the same as in the complete force profile in Fig. 9(a) for smaller colloids. This is the onset, where the channel center becomes stable against motion along the y axis and the colloid is constrained to the xz plane at $y = 0$. Further decreasing the aspect ratio w/h, the unstable and saddle fix points at $y \neq 0$ merge and vanish completely. Only the saddle fix point

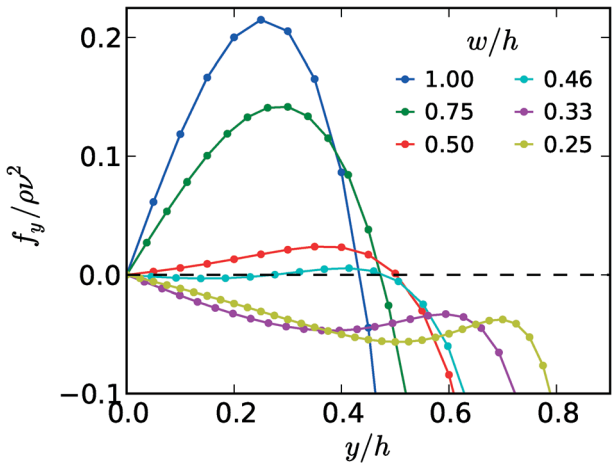

Fig. 5 Lift force f_y along the y-direction at $x = 0$ is plotted *versus* the y position of Re = 10 and $a/w = 0.4$. The different colors correspond to different aspect ratios w/h.

at $x = y = 0$ remains as illustrated in Fig. 3(c). Finally, we noted that at $w/h \approx 0.75$ the stable equilibrium position in the channel cross section switches from the diagonal to the x axis, which is not observed in Fig. 5.

We summarized the situation in the bifurcation diagram in Fig. 6, where we have plotted the equilibrium positions on the y axis *versus* the aspect ratio w/h. At sufficiently small w/h only the saddle fix point at $y = 0$ exists [Fig. 3(c)]. With increasing w/h, subcritical pitchfork bifurcation occurs. A second fix point appears which splits into the saddle and unstable fix points [Fig. 9(a)]. The latter ultimately merges with the fix point at $y = 0$ which becomes unstable [Fig. 3(b)]. This resulting situation is illustrated in the left inset for the whole cross section and with the stable fix point on the x axis. The stable fix point moves to the diagonal at $w/h \geq 0.75$. The regime of the subcritical pitchfork bifurcation is much more pronounced for smaller particles as illustrated in the

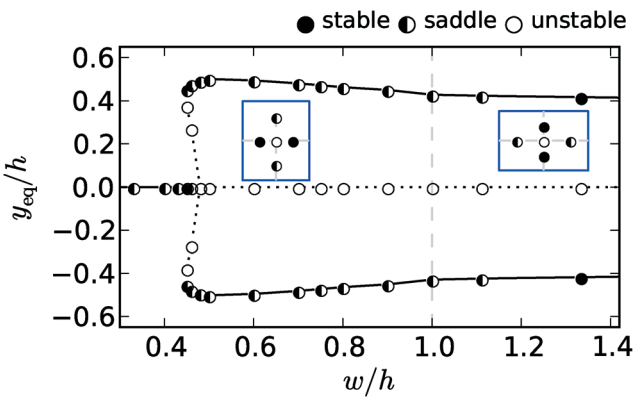

Fig. 6 Equilibrium positions along the y axis are plotted *versus* the channel aspect ratio w/h of Re = 10 and colloid radius $a/w = 0.4$. The equilibrium positions are categorized as stable, saddle, and unstable, using also their stability with respect to the x direction. The blue insets show typical equilibrium positions in the channel cross section for $w/h < 1$ (left) and for $w/h > 1.33$ (right).

inset of Fig. 7 of a colloid radius $a/w = 0.2$. The lift force profiles in this regime (see Fig. 7) even show that the subcritical transition to a single saddle fix point does not occur for small aspect ratios. This might be due to the fact that below $w/h = 0.4$ the flow profiles close to the wall are the same. Looking back to Fig. 6, at $w/h > 1$ (now the short main axis points along the y direction), the saddle fix point at non-zero y_{eq} first remains. It becomes stable at an aspect ratio $w/h \approx 1.33$ when the fix point on the diagonal vanishes. The situation is sketched in the right inset.

The basic features of the inertial lift force can be explained by considering the unperturbed flow field. In particular, the lift force depends on the curvature of the flow field.[6,11] Along the long channel axis (y direction), we observed the flow velocity shown in Fig. 2. As the channel height h increases, the flow profile in the center flattens considerably and the curvature strongly increases. The differences in the flow profiles of $w/h = 1$ and 0.75 are small, which corresponds to the modest decrease in the strength of the lift force shown in Fig. 5. At $w/h = 0.5$ the pronounced flattening of the flow profile sets in which marks the occurrence of the subcritical bifurcation and the strong changes in the lift force profiles shown in Fig. 5. Finally, we observed that the strength of the lift force in the x-direction also becomes weaker with decreasing aspect ratio w/h but the overall characteristics of the profile (two fix points) remain the same. Especially for aspect ratios $w/h \leq 0.5$, the lift force the in the x-direction does hardly change.

For many microfluidic applications, such as cytometry[36] or particle separation,[2] it is advantageous to ensure that particles are constrained to move in a plane so that they can easily be monitored in the focal plane of a microscope. Here we observed that as soon as the center position becomes a saddle point, particles will not leave the center plane any more since they always experience a force driving them back towards the plane. In Fig. 8, we plotted the necessary aspect ratio to constrain particles to the center plane. It becomes smaller with decreasing particle size and Reynolds number. For the particle sizes investigated here it is sufficient to choose $w/h < 0.4$ to ensure that the system is effectively two-dimensional. In the experiments, it was observed that with increasing Reynolds number some particles left the center plane,[36] which we cannot explain by our results. In Fig. 2a of ref. 36 particles are in close distance to each other. We therefore suspect that hydrodynamic interactions between particles, which are not included in our simulations, could be relevant for this effect.

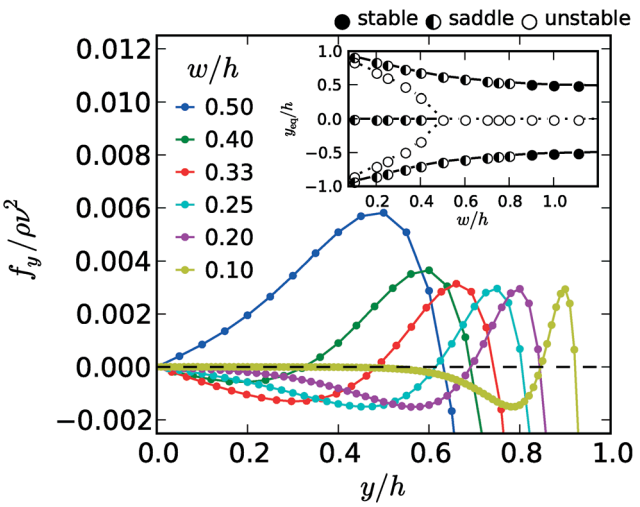

Fig. 7 Lift force f_y along the y direction at $x = 0$ is plotted *versus* the y position of Re = 10 and $a/w = 0.2$. The different colors correspond to different aspect ratios w/h. The inset shows the equilibrium positions along the y axis plotted *versus* the channel aspect ratio w/h. The equilibrium positions are categorized as stable, saddle, and unstable, using also their stability with respect to the x direction.

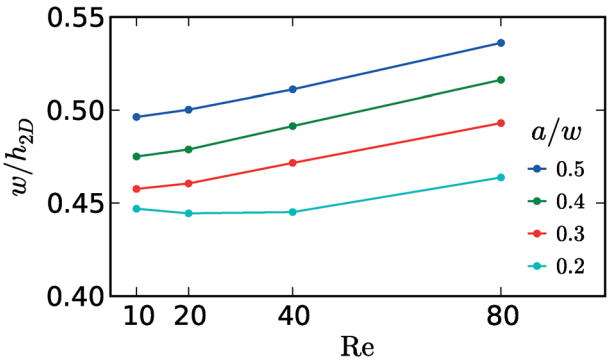

Fig. 8 Aspect ratio w/h_{2D} at which the center becomes a saddle fix point and the particles move in the center plane. w/h_{2D} is plotted *versus* Re for different particle sizes. The symbols are data points from the simulations.

4. Axial control of lift forces

In their experiments, Kim and Yoo applied an axial electric field which slows down particles relative to the Poiseuille flow.[18] As a result, particles are pushed towards the centerline. The observed migration can be rationalized with the Saffman force which is an inherent inertial force.[19] It acts perpendicular to a shear flow when particles are slowed down or sped up relative to the fluid flow. In their experiments, Kim and Yoo considered the flow with channel Reynolds numbers Re ≈ 0.05 well below unity. Our idea is to apply this concept to moderate Re and manipulate the inertial lift force using the additional Saffman force. We will show that with the help of an axial control force, we can modify the inertial lift force profile such that we can steer a particle to almost any desired position on the x axis.

For a particle of radius $a = 0.2w$ we observed without axial control the cross sectional force profile shown in Fig. 9(a). As discussed in the previous section we observed that a particle is pushed towards the $y = 0$ plane where it remains confined. When we applied an additional axial control force of $f_{ctl} = 2.5\rho v^2$, the force profile changed drastically [Fig. 9(b)]. In particular, the stable equilibrium position at $x/w \approx 0.46$ vanishes and the particle is focussed to the channel center regardless of its initial position.

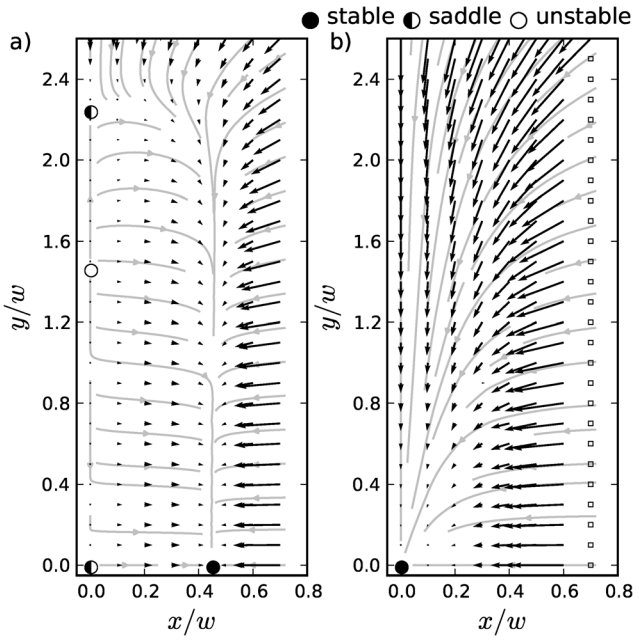

Fig. 9 Lift force profile of a/w = 0.2, Re = 10, w/h = 1/3 without the axial control (a) and with axial control force $f_{ctl} = 2.5\rho\nu^2$ (b).

We considered in the following a channel of aspect ratio w/h = 1/3 to ensure that the particle is confined to the y = 0 plane and focused on the lift force along the x direction. In Fig. 10 we plotted the inertial lift force profiles of several axial control forces f_{ctl}. For zero control force (green curve), the typical lift force profile occurs with the unstable equilibrium position at the center and the stable position half way between the channel center and the wall. When we applied the axial control force in the flow direction so that the particle is sped up relative to the flow (negative f_{ctl}), the lift force increases and the stable equilibrium position is pushed further towards the channel wall. The stable position moves closer to the center when we slowed down the particle with a positive control force f_{ctl} acting against the flow. The additional Saffman force decreases the lift force. Ultimately both

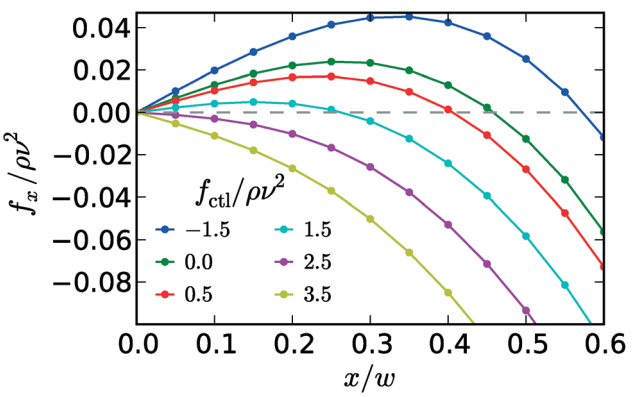

Fig. 10 Inertial lift force is plotted *versus* location x for different axial control forces f_{ctl} of Re = 10 and a/w = 0.2.

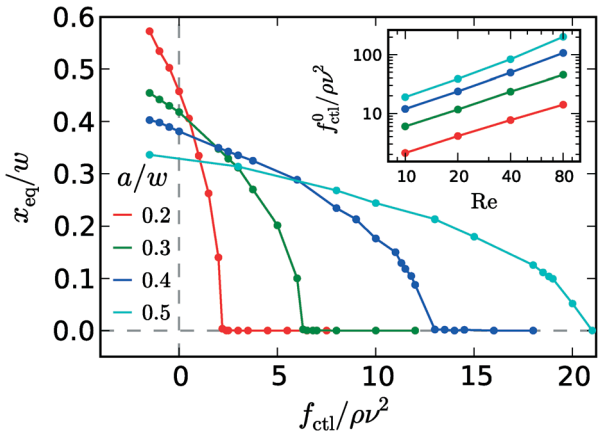

Fig. 11 Equilibrium position x_{eq} is plotted *versus* axial control force f_{ctl} for different particle radii a/w. The inset shows the minimum control force f^0_{ctl} needed to focus a particle to the channel center that is plotted *versus* Re for different particle sizes.

fix points merge and the particle position at the center is stabilized when the inertial force profile becomes completely negative. We also studied the change in the lift force of the fixed position x and found that it is nearly linear in the applied control forces. In Fig. 10 we already observe that the variation of the inertia lift force with the axial control force is the strongest close to the wall.

In Fig. 11 we plotted the stable equilibrium position x_{eq} *versus* f_{ctl} of different particle sizes. Starting from its uncontrolled value, the equilibrium position continuously shifts to zero as the control force increases. A negative control force moves x_{eq} towards the wall. In general, we observed that larger particles require larger control forces in order to move the equilibrium position. To analyze this effect further, we investigated the minimum control force f^0_{ctl} needed to steer a particle towards the channel center for different Reynolds numbers and particle sizes in the inset of Fig. 11. We observed that f^0_{ctl} strongly increases both with particle size and Reynolds number. When fitted to the power law, we obtained $f^0_{ctl} \propto \mathrm{Re}^{1.02}(a/w)^{2.60}$. This indicates that we can easily exploit an axial control force for particle sorting by size. For example, consider two particle types with sizes a/w = 0.2 and a/w = 0.3. While the small particle is well focussed to the channel center with a control force $f_{ctl} = 3\rho\nu^2$, the larger particle only changes its equilibrium position by about 10 %.

5. Feedback control

We have seen already in the previous section that a constant axial control force allows the manipulation and sorting of particles of different types. In the following, we will demonstrate how a simple feedback scheme adds additional control to the system and, in particular, increases particle throughput. We will present results where we simulated particle motion using the Langevin dynamics described in sect. 4.

We used a hysteretic control feedback scheme, which switches from no control to constant control depending on

the lateral particle position with the goal of keeping the particle close to the channel center. In concrete, we chose a target interval $[-b, b]$ for the x position of the particle. We switched the axial control force to a constant value f_0 when the particle is outside the target interval. The modified lift force profile drives the particle back to the channel center, and we switched off the control force until the particle leaves the target interval again. We show the resulting hysteretic control cycle of f_{ctl} in Fig. 12(a), which either acts in the positive or negative x direction. The applied control force changes not only the lift force profile but also the particle velocity along the channel axis as we demonstrate in Fig. 12(b). When the control is active, the particle slowed down compared to the uncontrolled motion.

Fig. 12(c) shows an example of a particle trajectory under the feedback scheme. The particle starts outside the target interval $[-b, b]$ and the lift force modified by the axial control force pulls it towards the channel centerline. As the particle reaches the centerline, the control is switched off and the particle is free to evolve. Since the centerline is an unstable fix point, the particle can leave the target interval and the control is activated again.

Performing feedback control instead of using a permanently applied control force has the advantage that the effect of control is reduced. In particular, feedback control gives an improved particle throughput while keeping the particle close to the centerline. In Fig. 13 we showed the mean particle speed (in units of the maximal flow speed u_0) as a function of the target width b for several control forces f_0. For the uncontrolled motion, v_{max} is the particle speed on the centerline and v_{eq} is the velocity at the equilibrium position. When the target interval contains the equilibrium position at $x = 0.46$, feedback control is not active. The particle stays at the equilibrium position and moves with v_{eq}. However, for smaller target widths feedback control sets in. We observed a mean particle velocity which is almost independent of the target width and the applied control force f_0. Only at $b = 0$, which means a permanently applied control force where the particle always stays in the center, does the mean velocity decrease. So, the particle throughput is the highest when feedback control is active.

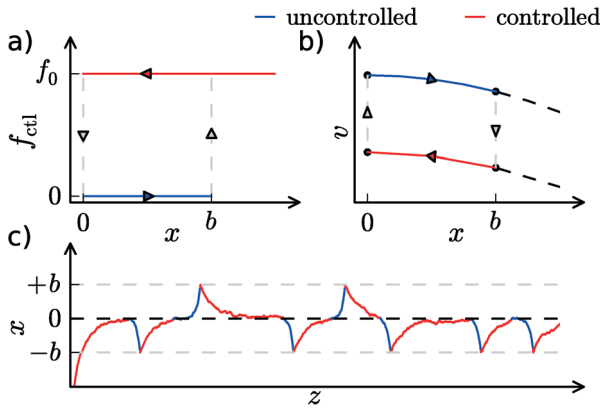

Fig. 12 (a) Schematic of the feedback control scheme. The axial control force f_0 is switched on when the particle leaves the target interval $[-b, b]$ and switched off once the particle reaches the centerline at $x = 0$. (b) Particle velocity in the target interval without and with control. (c) Example of a particle trajectory. The residence time on the centerline is determined by thermal fluctuations.

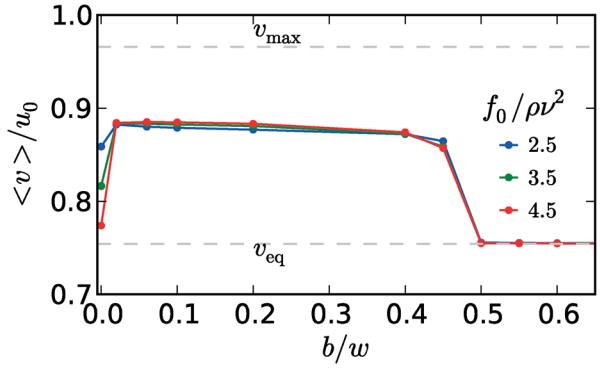

Fig. 13 Mean particle velocity $\langle v \rangle$ in units of the maximum Poiseuille flow speed u_0 plotted *versus* target width b. Different control forces f_0 within the hysteretic feedback control scheme are used. v_{max} is the particle speed on the centerline and v_{eq} is the velocity at the equilibrium position when no control acts.

6. Conclusion

Inertial microfluidics has proven to be particularly useful in applications such as particle steering and sorting which are important tasks in biomedical applications. In this paper, we provided further theoretical insights into inertial microfluidics using lattice Boltzmann simulations. We put special emphasis on controlling the particle motion either by designing the channel geometry or by applying an additional control force.

We first investigated the equilibrium positions in square and rectangular channels using lift force profiles and categorized them into stable, saddle, and unstable fix points. In square channels, the stable fix points either sit on the diagonals or the main axis of the cross section. This depends on particle size and Reynolds number and thereby offers the possibility to sort particles of different sizes. For rectangular channels we illustrated bifurcation scenarios of fix points situated on the long main axis. In particular, we showed that for sufficiently elongated channel cross section particles are pushed into a plane. Their dynamics becomes two-dimensional which simplifies the monitoring; and thereby control of particle motion in experiments.

We then demonstrated how an additional axial control force allows tuning of the stable equilibrium position, which moves towards the center with increasing force. Ultimately the stable position stays on the centerline when the force exceeds a threshold value which we identified for different particle sizes and Reynolds numbers. The strong dependence on these parameters allows separation of particles by size. Finally, we proposed a hysteretic feedback scheme using the axial control force to enhance particle throughput compared to the case when the control force is constantly applied.

The axial control force can be implemented by applying an external electric field along the channel axis which induces an electrophoretic force acting on the particle as demonstrated by Kim and Yoo.[18] Since the electric field can easily be tuned, the method introduced in this article to manipulate the lift force profile should be realizable in experiments, as well as to explore the proposed hysteretic feedback scheme.

We plan to extend our work to investigate the collective colloidal dynamics induced by the hydrodynamic interactions between particles. Here, the additional axial order such as particle trains develops.[37,38] Furthermore, it will be challenging to generalize our control methods to particle suspensions. The theoretical insights developed in this paper and future work on the collective dynamics will help to generate novel ideas for devices in biomedical applications based on inertial microfluidics.

Acknowledgements

We acknowledge support from the Deutsche Forschungsgemeinschaft in the framework of the Collaborative Research Center SFB 910.

References

1 S. C. Hur, A. J. Mach and D. Di Carlo, *Biomicrofluidics*, 2011, **5**, 022206.
2 A. J. Mach and D. Di Carlo, *Biotechnol. Bioeng.*, 2010, **107**, 302–311.
3 G. Guan, L. Wu, A. A. Bhagat, Z. Li, P. C. Chen, S. Chao, C. J. Ong and J. Han, *Sci. Rep.*, 2013, **3**, 1475.
4 J. S. Dudani, D. R. Gossett, T. Henry and D. Di Carlo, *Lab Chip*, 2013, **13**, 3728–3734.
5 G. Segré and A. Silberberg, *Nature*, 1961, **189**, 209–210.
6 D. Di Carlo, J. F. Edd, K. J. Humphry, H. A. Stone and M. Toner, *Phys. Rev. Lett.*, 2009, **102**, 094503.
7 D. Di Carlo, *Lab Chip*, 2009, **9**, 3038–3046.
8 Y. Kataoka and T. Inamuro, *Philos. Trans. R. Soc., A*, 2011, **369**, 2528–2536.
9 B. Chun and A. J. C. Ladd, *Phys. Fluids*, 2006, **18**, 031704.
10 J. Zhou and I. Papautsky, *Lab Chip*, 2013, 1121–1132.
11 J. P. Matas, J. F. Morris and E. Guazzelli, *Oil Gas Sci. Technol.*, 2004, **59**, 59–70.
12 H. Bruus, *Theoretical microfluidics*, Oxford University Press, 2007.
13 E. S. Asmolov, *J. Fluid Mech.*, 1999, **381**, 63–87.
14 B. P. Ho and L. G. Leal, *J. Fluid Mech.*, 1974, **65**, 365–400.
15 C. Prohm, M. Gierlak and H. Stark, *Eur. Phys. J. E*, 2012, **35**, 1–10.
16 M. MacDonald, G. Spalding and K. Dholakia, *Nature*, 2003, **426**, 421–424.
17 C. Prohm, F. Tröltzsch and H. Stark, *Eur. Phys. J. E*, 2013, **36**, 1–13.
18 W. Y. Kim and J. Y. Yoo, *Lab Chip*, 2009, **9**, 1043–1045.
19 P. G. Saffman, *J. Fluid Mech.*, 1965, **22**, 384–400.
20 K. Aström and R. Murray, *Feedback Systems: An Introduction for Scientists and Engineers*, Princeton University Press, 2010.
21 A. Jonáš and P. Zemánek, *Electrophoresis*, 2008, **29**, 4813–4851.
22 G. J. Wuite, S. B. Smith, M. Young, D. Keller and C. Bustamante, *Nature*, 2000, **404**, 103–106.
23 M. D. Wang, H. Yin, R. Landick, J. Gelles and S. M. Block, *Biophys. J.*, 1997, **72**, 1335–1346.
24 R. W. Applegate Jr, D. N. Schafer, W. Amir, J. Squier, T. Vestad, J. Oakey and D. W. Marr, *J. Opt. A: Pure Appl. Opt.*, 2007, **9**, S122.
25 X. Wang, S. Chen, M. Kong, Z. Wang, K. D. Costa, R. A. Li and D. Sun, *Lab Chip*, 2011, **11**, 3656–3662.
26 M. S. Munson, J. M. Spotts, A. Niemistö, J. Selinummi, J. G. Kralj, M. L. Salit and A. Ozinsky, *Lab Chip*, 2010, **10**, 2402–2410.
27 B. Dünweg and A. J. Ladd, *Advances in Polymer Science*, Springer, Berlin Heidelberg, 2008, pp. 1–78.
28 C. K. Aidun and J. R. Clausen, *Annu. Rev. Fluid Mech.*, 2010, **42**, 439–472.
29 X. Shan and H. Chen, *Phys. Rev. E: Stat. Phys., Plasmas, Fluids, Relat. Interdiscip. Top.*, 1993, **47**, 1815–1819.
30 T. Inamuro, *Fluid Dynam. Res.*, 2012, **44**, 024001.
31 *The Palabos project*, 2013, http://www.palabos.org.
32 G. Le and J. Zhang, *Phys. Rev. E: Stat., Nonlinear, Soft Matter Phys.*, 2009, **79**, 026701.
33 T. Krüger, F. Varnik and D. Raabe, *Phys. Rev. E: Stat., Nonlinear, Soft Matter Phys.*, 2009, **79**, 046704.
34 P. Kloeden and E. Platen, *Numerical Solution of Stochastic Differential Equations*, Springer, 2011.
35 D. R. Gossett, H. T. K. Tse, J. S. Dudani, K. Goda, T. A. Woods, S. W. Graves and D. Di Carlo, *Small*, 2012, **8**, 2757–2764.
36 S. C. Hur, H. T. K. Tse and D. Di Carlo, *Lab Chip*, 2010, **10**, 274–280.
37 W. Lee, H. Amini, H. A. Stone and D. Di Carlo, *Proc. Natl. Acad. Sci. U. S. A.*, 2010, **107**, 22413–22418.
38 K. J. Humphry, P. M. Kulkarni, D. A. Weitz, J. F. Morris and H. A. Stone, *Phys. Fluids*, 2010, **22**, 081703.